

Size effects in the magneto-optical response of Co nanoparticles

C. Clavero,* A. Cebollada, and G. Armelles

Instituto de Microelectrónica de Madrid—IMM (CNM-CSIC), Isaac Newton 8-PTM, E-28760 Tres Cantos, Madrid, Spain

Y. Huttel

Instituto de Ciencia de Materiales de Madrid (ICMM-CSIC), 28049 Cantoblanco, Madrid, Spain

J. Arbiol, F. Peiró, and A. Cornet

EME Electronic Materials and Engineering, Department Electronics, University of Barcelona, Martí i Franquès 1, 08028 Barcelona, Spain

(Received 6 September 2004; revised manuscript received 22 December 2004; published 19 July 2005)

A study of the magneto-optical (MO) spectral response of Co nanoparticles embedded in MgO as a function of their size and concentration in the spectral range from 1.4 to 4.3 eV is presented. The nanoparticle layers were obtained by sputtering at different deposition temperatures. Transmission electron microscopy measurements show that the nanoparticles have a complex structure which consists of a crystalline core having a hexagonal close-packed structure and an amorphous crust. Using an effective-medium approximation we have obtained the MO constants of the Co nanoparticles. These MO constants are different from those of continuous Co layers and depend on the size of the crystalline core. We associate these changes with the size effect of the intraband contribution to the MO constants, related to a reduction of the relaxation time of the electrons into the nanoparticles.

DOI: [10.1103/PhysRevB.72.024441](https://doi.org/10.1103/PhysRevB.72.024441)

PACS number(s): 75.75.+a, 75.70.Ak, 78.67.-n

I. INTRODUCTION

The physical properties of nanoparticles may differ considerably from the bulk properties of the constituent materials. These differences arise fundamentally from the fact that in the nanoparticles a relatively large fraction of the atoms are placed in the surface, and also from their finite size which breaks the periodicity of the lattice;¹⁻³ these features induce changes in the electronic structure which are reflected in changes of the optical, magnetic, and magneto-optical (MO) properties. The changes of the optical response of these systems have been widely studied as a function of the size and concentration of nanoparticles.³⁻⁵ Also there has been a strong effort to investigate the magnetic properties and interactions between the nanoparticles depending on their size and relative distances.⁶⁻⁹ In this field surprising properties have been discovered, like the increase of the magnetic moment per atom in free Co, Fe, and Ni clusters exceeding the bulk value,^{10,11} the enhancement of the magnetic anisotropy^{2,12} attributed to surface effects in the nanoparticles, the doubling of the orbital magnetic moment in Fe nanoparticles,¹³ or the onset of ferromagnetic behavior in Pd nanoparticles.¹⁴ However, less effort has been devoted to the study of how the MO response is influenced by the size and concentration of the nanoparticles embedded in a dielectric matrix.^{1,15-18}

In this paper we present a study of the MO response of thin layers of Co nanoparticles embedded in MgO. Using the effective-medium approximation, we obtain the MO properties of the Co nanoparticles, which differ considerably from those of Co bulk material and depend on the size of the crystalline core. We associate these differences with a size effect in the intraband contribution to the MO constants.

After a brief description of the deposition and experimental characterization techniques in Sec. II, we describe in Sec. III the morphological evolution of the Co nanoparticles as a function of the deposition temperature. Finally, in Sec. IV we study how the morphological nanoparticle parameters depend on the MO spectral response of the system.

II. EXPERIMENT

The samples were grown in an ultrahigh-vacuum multi-chamber system equipped with sputtering and laser ablation facilities. The Co deposition was performed by triode sputtering on a Si substrate with a 1000 Å Si₃N₄ buffer layer, at different deposition temperatures (200, 400, 550, and 700 °C), with a Co deposition time of 2 min in all the samples and at a deposition rate of 15 Å/min. Subsequently to the Co growth, a 30-Å-thick MgO overlayer was deposited at room temperature by normal-incidence pulsed laser deposition from a monocrystalline MgO target. The structural characterization was done by x-ray reflectivity (XRR) and transmission electron microscopy (TEM). XRR experiments were performed in a standard four-circle diffractometer with Cu K α radiation to estimate the thickness of the layers. TEM images were obtained in cross-section configuration, plan-view energy-filtered TEM (EFTEM) (from electron energy loss spectroscopy) and plan-view bright-field TEM (BFTEM). The MO properties were studied using a polar Kerr MO spectrometer described elsewhere¹⁹ in the spectral range from 1.4 to 4.3 eV. None of the studied structures exhibited superparamagnetic character, as confirmed by transverse Kerr measurements, with the observation of clear hysteresis loops and with clear coercivity.

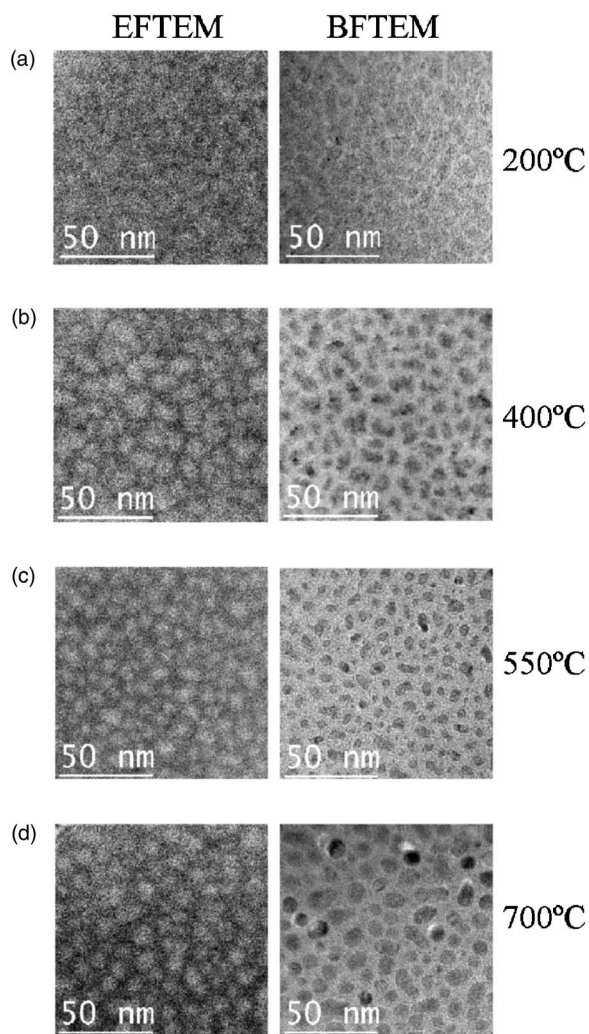


FIG. 1. EFTEM (left) and BFTEM (right) plan-view micrographs of the samples grown at 200 (a), 400 (b), 550 (c), and 700 °C (d). EFTEM images are obtained from the $M_{2,3}$ line of Co, revealing all the Co present in the sample, while BFTEM images display only the crystalline Co.

III. MORPHOLOGICAL EVOLUTION OF THE LAYERS

It is well known that deposition temperature is a crucial parameter that determines the growth mode in both epitaxial and heteroepitaxial systems. Examples are the two-dimensional (2D) vs three-dimensional (3D) growth modes as deposition temperature increases for the heteroepitaxy of Fe on MgO (Ref. 20) and *c*-sapphire (Ref. 21) or Co on AlN.²² In all cases, deposition at moderate temperatures reduces surface diffusion leading to a 2D growth mode, while increasing deposition temperature leads to a gradual 3D morphology.

In this work we observe the same process for Co deposition on Si_3N_4 , with 2D-like growth at low deposition temperatures and 3D-like nanoparticle growth at elevated temperatures. Then, if the amount of deposited material is small, the nanoparticle concentration can be controlled by changing the deposition temperature. This is illustrated in Fig. 1, where TEM images corresponding to the samples grown at

200, 400, 550, and 700 °C are shown. In the left column of Fig. 1 EFTEM plan-view micrographs are presented. In this configuration all the electrons with an energy loss corresponding to the $M_{2,3}$ line of Co are collected (crystalline and noncrystalline Co) so we can obtain the spatial Co localization in the layer. As can be observed, as we increase the deposition temperature the Co atoms aggregate to form nanoparticles and the concentration of Co in the layers decreases. This behavior corresponds to a change of the growth mode from 2D to 3D as the deposition temperature increases. In particular, the sample grown at the lowest temperature (200 °C) is a nearly continuous layer of Co, whereas in the sample grown at 550 or 700 °C isolated Co nanoparticles are clearly observed. In Fig. 2(a) we present the evolution with the growth temperature of the concentration of Co nanoparticles in the layers together with the mean in-plane diameter of the nanoparticles obtained using this technique [Fig. 2(b)].

In the right column of Fig. 1 we show the corresponding BFTEM planar-view micrographs sensitive only to the crystalline Co in the nanoparticles. We can observe that for all the samples except for the one grown at 700 °C, the diameters of the nanoparticles are lower than those extracted from the EFTEM images. These results suggest that the nanoparticles are made of a crystalline hcp core surrounded by an amorphous crust, the thickness of this amorphous crust decreasing as we increase the deposition temperature. In Fig. 2(b) the mean nanoparticle diameters extracted from EFTEM and BFTEM images are plotted as a function of the growth temperature; the amorphous crust is made of different stoichiometric Co oxides (CoO and Co_3O_4).

The results of cross-section TEM also display the same behavior as seen in the planar-view micrographs and no reaction between the deposited Co and the Si_3N_4 buffer layers was detected. The thickness of the Co nanoparticle layers and MgO capping layer obtained with this technique and by means of XRR is similar. The thickness of the nanoparticle layers range from 3 nm in the sample grown at 200 °C with the higher Co concentration to 4 nm in the sample grown at 700 °C, whereas the thickness of the MgO capping layer was found to be ≈ 3 nm in all the samples. A sketch of the nanoparticle plus crust structure is shown in Fig. 2(c).

IV. CONCENTRATION, SIZE, AND CRYSTALLINE-QUALITY DEPENDENCE OF THE MO SPECTRAL RESPONSE

In Fig. 3 we present the nondiagonal real and imaginary parts of the effective dielectric tensor (MO constants) corresponding to the layers consisting of Co nanoparticles grown at different temperatures and embedded in a MgO matrix. The MO constants were obtained from the experimental polar Kerr rotation (θ) and ellipticity (ϵ) spectra of the samples, which for thin enough layers are related to the nondiagonal components (ϵ_{xy}) as follows:²³

$$\Phi_k = \theta + i\epsilon = a \text{Re}(\epsilon_{xy}) + b \text{Im}(\epsilon_{xy}) \quad (1)$$

where the complex coefficients a and b depend on the optical properties and the thickness of the different layers that form the structure, which is schematized in Fig. 2(c).

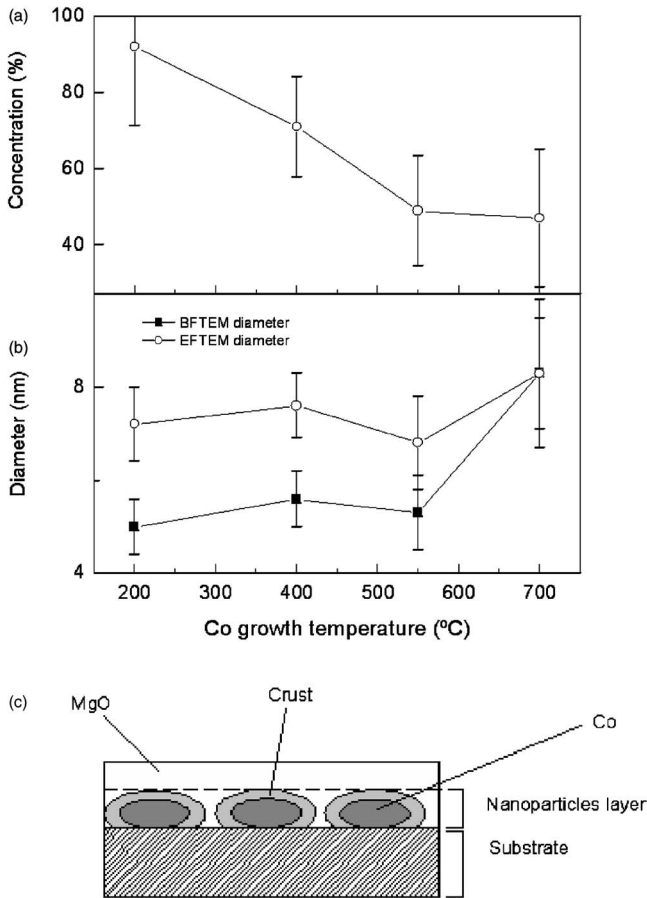


FIG. 2. (a) Concentration of Co nanoparticles and (b) nanoparticle mean diameter measured by EFTEM and BFTEM as a function of the Co deposition temperature. (c) Sketch of the sample structure.

As can be observed in Fig. 3 the values of the real part of the MO constants in the ultraviolet range are similar for all the samples. On the contrary in the visible and near-infrared ranges there is a dependence on the growth temperature; even a change of sign is observed as the deposition temperature is increased. On the other hand, the imaginary part of the MO constant is less affected by the deposition temperature. For the samples grown at 200, 400, and 550 °C particle concentration is in principle the main parameter that changes and therefore should play an important role in the evolution of the MO constant observed in Fig. 3.

As the size of the nanoparticles is much smaller than the wavelength of the incident light we can analyze the evolution of the MO constants as a function of the concentration using an effective-medium approximation. In this approximation the effective dielectric tensor ϵ_e of a composite material consisting of particles randomly distributed in a matrix depends on the dielectric tensors of the particles and matrix, concentration and shape of the particles^{15,24,25} as follows:

$$\epsilon_e - \epsilon_0 = \langle (1 - \delta\epsilon\Gamma)^{-1} \rangle^{-1} \langle (1 - \delta\epsilon\Gamma)^{-1} \delta\epsilon \rangle \quad (2)$$

where $\delta\epsilon = \epsilon(r) - \epsilon_0$, $\epsilon(r)$ is the dielectric tensor of the matrix or particle material at r , ϵ_0 is an arbitrary defined reference

dielectric tensor, Γ is a tensor depending on the shape of the particles, and the angular brackets indicate that a volume average is taken.

Two fundamental approximations can be made depending on the reference tensor ϵ_0 used: the Bruggeman and Maxwell-Garnett approximations. In the Bruggeman approximation the reference dielectric tensor ϵ_0 is taken equal to $\epsilon_0 = \epsilon_e$ and the expression (2) is reduced to

$$\langle (1 - \delta\epsilon\Gamma)^{-1} \delta\epsilon \rangle = 0. \quad (3)$$

Therefore, in principle no distinction is made between the matrix material and the particle material. This approximation should be used to treat systems with a morphology where no clear assignment of which is the matrix material could be done. On the contrary in the Maxwell-Garnett approximation the matrix material determines the choice of the reference dielectric tensor ϵ_0 as this one is taken equal to that of the matrix $\epsilon_0 = \epsilon_m$, and is more appropriate to treat systems with a morphology where such assignment of the matrix material is possible.

In Figs. 4(a) and 4(b) we present the calculated MO constants of a composite material made of Co and MgO for different Co concentrations using the Bruggeman and Maxwell-Garnett approximations, respectively. The MgO has been considered as the matrix material; therefore the shape factor in the Bruggeman approximation for MgO has been taken as that of spherical particles, whereas the shape factor for Co is taken as that of disklike-shaped particles (with shape factors $L_x = L_y = 0.236$ and $L_z = 0.527$) which corresponds to the shape observed in the TEM micrographs shown in Fig. 1. In these calculations we have used the MO constants of Co extracted from the sample grown at 200 °C, which has a very high concentration of Co (92%), and the refractive index obtained from ellipsometry measurements on thin Co layers. As can be observed, for this range of concentration, the evolution of the MO constants with the concentration obtained in these two approximations is very different. We would like to point out that for such concentrations, if Co is considered as the matrix material, both approximations give similar results, and are also very similar to the evolution obtained using the Bruggeman approximation presented in Fig. 4(a).

Also in these figures we present the experimental results for samples grown at 200, 400, and 550 °C which have similar Co nanoparticle size but different Co concentration. As can be observed the experimental results agree better with the simulations performed within the Maxwell-Garnett approximation than using the Bruggeman approximation. These results are consistent with the morphology of the layers observed in TEM for samples grown at 400 and 550 °C where isolated Co nanoparticles embedded in a MgO matrix are seen. Therefore, they should behave more like a system of disklike-shaped Co nanoparticles embedded in a MgO matrix (Maxwell-Garnett approximation), than a composite material made of Co and MgO (Bruggeman approximation).

However, neither of the two models reproduces the differences observed between the samples grown at 550 and 700 °C, which have similar Co concentrations but different

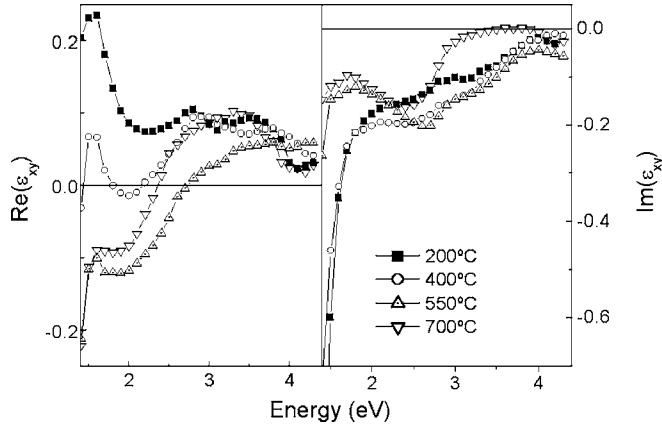


FIG. 3. Experimental MO constants of the different layers consisting of Co nanoparticles deposited at 200, 400, 550, and 700 °C and embedded in MgO.

nanoparticle mean crystalline core sizes. To clarify the dependence of the MO constants of the nanoparticles with their size, we present in Fig. 5 the MO constants of Co in the nanoparticles for the different samples. They were obtained, from the experimental MO constants of the nanoparticles layers (Co nanoparticles+MgO) using the Maxwell-Garnett approximation as follows:

$$\epsilon_{xy}^{\text{Co}} = \frac{\epsilon_{xy}^{\text{eff}}}{f} \left(1 + (1-f) \frac{(\epsilon_{xx}^{\text{Co}} - \epsilon_{xx}^{\text{MgO}}) L_x}{\epsilon_{xx}^{\text{MgO}}} \right)^2 \quad (4)$$

where $\epsilon_{xy}^{\text{Co}}$ and $\epsilon_{xy}^{\text{eff}}$ are the MO constants of the Co in the nanoparticles and in the nanoparticle layer (Co nanoparticles+MgO), respectively, $\epsilon_{xx}^{\text{Co}}$ and $\epsilon_{xx}^{\text{MgO}}$ are the diagonal elements of the dielectric tensor of Co and MgO, f is the nanoparticle concentration, and L_x the component of the depolarization tensor, which depends on the shape of the nanoparticle.¹⁵ The nanoparticle concentration and shape were obtained from TEM measurements; we have assumed that the optical constants do not differ much from one sample to another, as deduced from ellipsometry measurements carried out on thin layers of Co grown at different temperatures under identical conditions. For comparison, also the MO constants of a 420-Å-thick Co continuous layer grown at room temperature (RT) are shown in Fig. 5. At first glance large differences are found between the MO constants of bulk Co (continuous layer) and the Co in the nanoparticle layers, with a strong decrease of the real part and a change of sign in the imaginary part. Moreover, the MO constants of Co obtained from the results of the samples grown at 200, 400, and 550 °C are very similar, and different from the MO constant obtained from the results of the sample grown at 700 °C. We attribute these differences to changes in nanoparticle size and crystalline quality.

The optical and MO properties of metallic bulk systems are related to intraband (owing to conduction electrons in the material) and interband contributions (due to interband transitions). The intraband contribution to the dielectric tensor can be described using a Drude model²⁶ as follows:²⁷

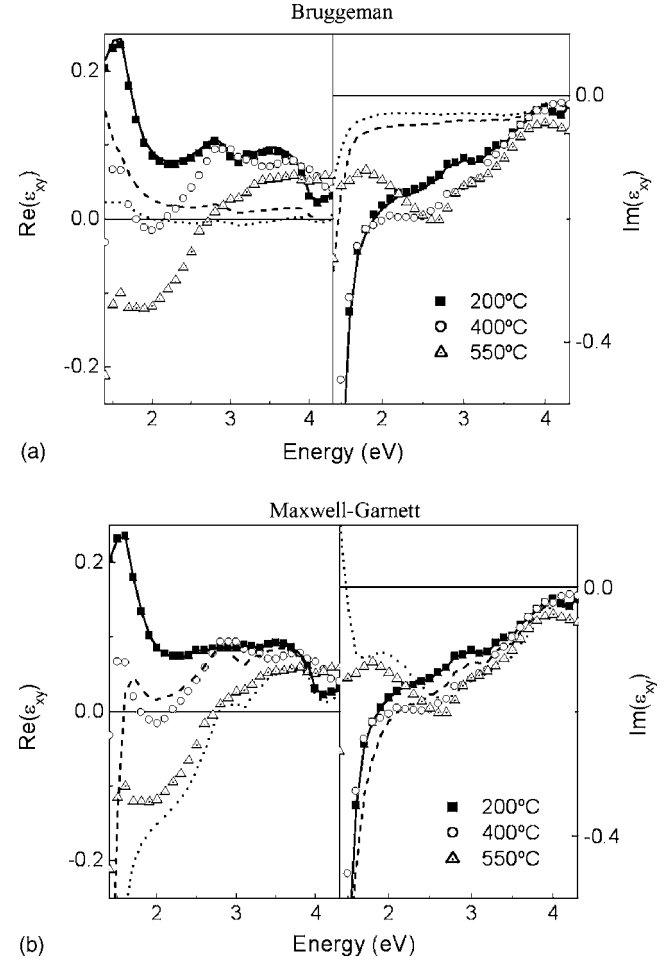


FIG. 4. Experimental (symbols) and fits for the MO constants corresponding to the nanoparticle layers of samples grown at 200 (continuous line), 400 (dashed line), and 550 °C (dotted line) calculated by means of (a) the Bruggeman and (b) the Maxwell-Garnett approximation.

$$\epsilon_{xx}^d(\omega) = 1 + i \frac{(1 - i\omega\tau)\omega_p^2\tau}{\omega[(1 - i\omega\tau)^2 + (\omega_c\tau)^2]},$$

$$\epsilon_{zz}^d(\omega) = 1 + i \frac{\omega_p^2\tau}{\omega(1 - i\omega\tau)},$$

$$\epsilon_{xy}^d(\omega) = \frac{\omega_c(\omega_p\tau)^2}{\omega[(1 - i\omega\tau)^2 + (\omega_c\tau)^2]}, \quad (5)$$

where $\omega_p = \sqrt{\frac{4\pi n e^2}{m}}$ is the plasma frequency, $\omega_c = \frac{eB}{mc}$ is the cyclotron frequency, and τ is the relaxation time of the electrons, which depends on the electron-electron, electron-phonon, and electron-defect scattering contributions.³

The thick continuous lines in Fig. 5 represent calculated MO constants given by Eq. (5) with the parameters obtained for Co by Krinchik^{28,29} ($\omega_p = 9.74$ eV, $\omega_c = 0.089$ eV, and $\tau = 0.632$ eV). As can be observed, with these parameters, a good agreement is obtained between the experimental results and the values given by Eq. (5); the remaining differences can be attributed to the interband contributions.

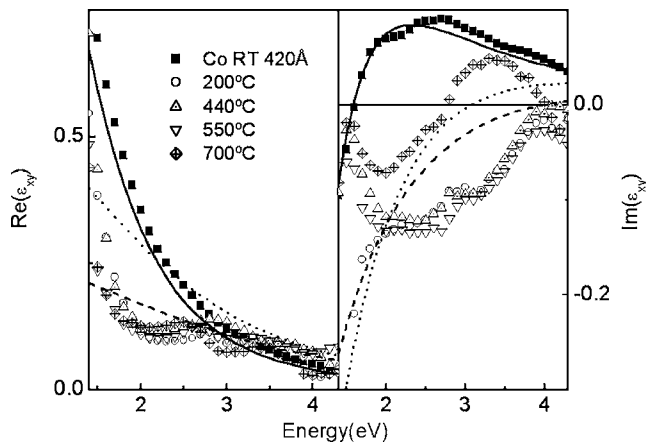


FIG. 5. MO constants of the Co that is part of the different nanoparticle thin layers deposited at 200, 400, 550, and 700 °C, together with the MO constants of a 420-Å-thick cobalt sample grown at RT (divided by 2). The continuous, dotted, and dashed lines correspond to the intraband contribution obtained using the Drude model and with $\tau=0.632$, 0.32, and 0.25 eV.

In granular layers we should expect that some of these Drude parameters might change, in particular the relaxation time related to the electron mean free path⁴ which is considerably reduced due to the breaking of the lattice periodicity and the collisions of the electrons with the surface of the nanoparticles. The dependence of the relaxation time on the size of the nanoparticles can be expressed as³⁻⁵

$$\frac{1}{\tau} = \frac{1}{\tau_0} + \frac{A}{R} \quad (6)$$

where R is the radius of the nanoparticle and A is a constant, which depends on the material and on the shape of the nanoparticles. A decrease of the relaxation time as the size of the nanoparticles decreases is, therefore, expected.

We have shown in the TEM micrographs that the Co nanoparticles consist of a crystalline core and an amorphous crust whose thickness decreases as the deposition temperature increases. The diameter of the crystalline core [Fig. 2(b)] is approximately the same for the samples grown at 200, 400, and 550 °C (around 5.2 nm), but larger for the sample grown at 700 °C (8.3 nm). Such a difference of the crystalline size can be an important factor in the MO constants of the Co in the nanoparticles, specially knowing that these constants are very similar in samples with the same crystalline size. For example, the dashed line in Fig. 5 represents the MO constant given by Eq. (5) and using the Krinchik parameters for Co but decreasing the relaxation

time to 0.25 eV. The calculated MO constants are similar to the MO constant of the samples grown at 200, 400, and 550 °C with some differences, in particular in the region between 1.4 and 2 eV, which are not well reproduced by this model. These differences can be attributed to interband transitions, which may be affected by the size and crystalline quality of the nanoparticles. In particular Co has a strong interband transition around 1 eV,³⁰ which is not taken into account in this model. On the other hand the crystalline size of the nanoparticles in the sample grown at 700 °C is larger and therefore the relaxation time should be higher. The dotted line in Fig. 5 represents the resulting MO constant obtained with a relaxation time of 0.32 eV [this relaxation time was obtained using Eq. (6), with values of τ_0 obtained from bulk and the constant A obtained from the sample grown at 200 °C]. As can be observed we can reproduce the evolution of the MO constant of Co in the nanoparticles assuming that the crystalline core size determines the relaxation time of the electrons.

In conclusion, the MO response of thin layers of Co nanoparticles embedded in a MgO matrix has been studied. The samples were grown by sputtering at different deposition temperatures. As the deposition temperature is increased the growth mode changes gradually from a bidimensional to a three-dimensional fashion, producing layers with different concentrations of nanoparticles. The nanoparticles consist of a crystalline core surrounded by an amorphous crust, the size of the crystalline core ranging from 5 to 8 nm. The MO response of the Co nanoparticle layer depends on two important structural parameters: the nanoparticle concentration and their crystalline core size. The evolution of the MO constants of the nanoparticle layers (Co nanoparticles+MgO) as a function of the nanoparticle concentration can be described using the Maxwell-Garnett approximation. The calculations reproduce the intensity and features of the experimental spectra. We have also observed changes in the MO response when the crystalline size of the nanoparticles decreases; part of these changes may be related to a decrease of the relaxation time of the electrons in the Co nanoparticles induced by a reduction of the electron mean free path due to the size of the nanoparticles.

ACKNOWLEDGMENTS

This work was partially financed by the Spanish Commission of Science and Technology and Comunidad de Madrid. Y.H. acknowledges the Consejo Superior de Investigaciones Científicas (CSIC) and the Ramón y Cajal program for financial support.

*Electronic address: cesarcl@imm.cnm.csic.es

¹B. Kalska, J. J. Paggel, P. Fumagalli, H. Hilgendorff, and M. Giersig, *J. Appl. Phys.* **92**, 7481 (2002).

²F. Luis, J. M. Torres, L. M. García, J. Bartolomé, J. Stankiewicz, F. Petroff, F. Fettar, J. L. Maurice, and A. Vaurès, *Phys. Rev. B*

65, 094409 (2002).

³N. Del Fatti, F. Vallée, C. Flytzanis, Y. Hamanaka, and A. Nakamura, *Chem. Phys.* **251**, 215 (2000).

⁴U. Kreibing and M. Vollmer, *Optical Properties of Metal Clusters* (Springer, Berlin, 1995).

- ⁵S. Norrman, T. Andersson, C. G. Granqvist, and O. Hunderi, *Phys. Rev. B* **18**, 674 (1978).
- ⁶M. Demand, M. Hehn, K. Ounadjela, J. V. Kim, A. Vagov, and R. L. Stamps, *J. Appl. Phys.* **85**, 5498 (1999).
- ⁷F. Luis, F. Petroff, J. M. Torres, L. M. García, J. Bartolomé, J. Carrey, and A. Vaurès, *Phys. Rev. Lett.* **88**, 217205 (2002).
- ⁸J. F. Löffler, H. B. Braun, and W. Wagner, *Phys. Rev. Lett.* **85**, 1990 (2000).
- ⁹A. Hernando, *J. Phys.: Condens. Matter* **11**, 9455 (1999).
- ¹⁰J. P. Bucher, D. C. Douglass, and L. A. Bloomfield, *Phys. Rev. Lett.* **66**, 3052 (1991).
- ¹¹S. E. Apsel, J. W. Emmert, J. Deng, and L. A. Bloomfield, *Phys. Rev. Lett.* **76**, 1441 (1996).
- ¹²M. Respaud, J. M. Broto, H. Rakoto, A. R. Fert, L. Thomas, B. Barbara, M. Verelst, E. Snoeck, P. Lecante, A. Mosset, J. Osuna, T. O. Ely, C. Amiens, B. Chaudret, *Phys. Rev. B* **57**, 2925 (1998).
- ¹³K. W. Edmonds, C. Binns, S. H. Baker, S. C. Thornton, C. Norris, J. B. Goedkoop, M. Finazzi, and N. B. Brookes, *Phys. Rev. B* **60**, 472 (1999).
- ¹⁴B. Sampedro, P. Crespo, A. Hernando, R. Litrán, J. C. Sánchez López, C. López Cartes, A. Fernández, J. Ramírez, J. González Calbet, and M. Vallet, *Phys. Rev. Lett.* **91**, 237203 (2003).
- ¹⁵J. L. Menéndez, B. Bescós, G. Armelles, R. Serna, J. Gonzalo, R. Doole, A. K. Petford-Long, and M. I. Alonso, *Phys. Rev. B* **65**, 205413 (2002).
- ¹⁶Z. S. Jiang, G. J. Jin, J. T. Ji, H. Sang, Y. W. Du, S. M. Zhou, Y. D. Wang, and L. Y. Chen, *J. Appl. Phys.* **78**, 439 (1995).
- ¹⁷J. L. Dormann, D. Fiorani, F. Giammaria, and F. Lucari, *J. Appl. Phys.* **69**, 5130 (1991).
- ¹⁸R. Carey, D. M. Newman, and B. W. J. Thomas, *Thin Solid Films* **129**, 231 (1985).
- ¹⁹W. S. Kim, M. Aderholz, and W. Kleemann, *Meas. Sci. Technol.* **4**, 1275 (1993).
- ²⁰C. Martínez Boubeta, E. Navarro, A. Cebollada, F. Briones, F. Peiró and A. Cornet, *J. Cryst. Growth* **226**, 223 (2001).
- ²¹J. L. Menéndez, G. Armelles, C. Quintana, and A. Cebollada, *Surf. Sci.* **482-485**, 1135 (2001).
- ²²Y. Huttel, H. Gómez, C. Clavero, A. Cebollada, G. Armelles, E. Navarro, M. Ciria, L. Benito, J. I. Arnaudas, and A. J. Kellock, *J. Appl. Phys.* **96**, 1666 (2004).
- ²³S. Visnovský, M. Nývlt, V. Prosser, R. Lopusník, R. Urban, J. Ferré, G. Péniard, D. Renard, and R. Krishnan, *Phys. Rev. B* **52**, 1090 (1995).
- ²⁴D. Stroud, *Phys. Rev. B* **12**, 3368 (1975).
- ²⁵J. S. Ahn, K. H. Kim, T. W. Noh, D.-H. Riu, K. H. Boo, and H.-E. Kim, *Phys. Rev. B* **52**, 15244 (1995).
- ²⁶P. B. Johnson and R. W. Christy, *Phys. Rev. B* **6**, 4370 (1972).
- ²⁷T. K. Xia, P. M. Hui, and D. Stroud, *J. Appl. Phys.* **67**, 2736 (1990).
- ²⁸G. S. Krinchik, *J. Appl. Phys.* **35**, 1089 (1964).
- ²⁹R. Carey and B. W. J. Thomas, *J. Phys. D* **7**, 2362 (1974).
- ³⁰G. Y. Guo and H. Ebert, *Phys. Rev. B* **50**, 10377 (1994).